

Generation of Ligand-Based Pharmacophore Model and Virtual Screening for Identification of Novel Tubulin Inhibitors with Potent Anticancer Activity

Yi-Kun Chiang,^{†,§} Ching-Chuan Kuo,^{‡,△} Yu-Shan Wu,^{▽,△} Chung-Tong Chen,[§] Mohane Selvaraj Coumar,[§] Jian-Sung Wu,[§] Hsing-Pang Hsieh,[§] Chi-Yen Chang,[‡] Huan-Yi Jseng,[§] Ming-Hsine Wu,[§] Jui-Shyang Leou,[§] Jen-Shin Song,[§] Jang-Yang Chang,[‡] Ping-Chiang Lyu,[†] Yu-Sheng Chao,[§] and Su-Ying Wu^{*,§}

[†]Institute of Bioinformatics and Structural Biology, National Tsing Hua University, Hsinchu 300, Taiwan, Republic of China, [‡]National Institute of Cancer Research, National Health Research Institutes, Tainan 704, Taiwan, Republic of China, [§]Division of Biotechnology and Pharmaceutical Research, National Health Research Institutes, 35 Keyan Road, Zhunan, Miaoli County 350, Taiwan, Republic of China, and [▽]Department of Chemistry, Tunghai University, 181 Taichung Harbor Road Sec. 3, Taichung 407, Taiwan, Republic of China. [△]These authors contributed equally.

Received December 29, 2008

A pharmacophore model, Hypo1, was built on the basis of 21 training-set indole compounds with varying levels of antiproliferative activity. Hypo1 possessed important chemical features required for the inhibitors and demonstrated good predictive ability for biological activity, with high correlation coefficients of 0.96 and 0.89 for the training-set and test-set compounds, respectively. Further utilization of the Hypo1 pharmacophore model to screen chemical database in silico led to the identification of four compounds with antiproliferative activity. Among these four compounds, **43** showed potent antiproliferative activity against various cancer cell lines with the strongest inhibition on the proliferation of KB cells ($IC_{50} = 187$ nM). Further biological characterization revealed that **43** effectively inhibited tubulin polymerization and significantly induced cell cycle arrest in G₂-M phase. In addition, **43** also showed the in vivo-like anticancer effects. To our knowledge, **43** is the most potent antiproliferative compound with antitubulin activity discovered by computer-aided drug design. The chemical novelty of **43** and its anticancer activities make this compound worthy of further lead optimization.

Introduction

Microtubules are cytoskeletal filaments consisting of α/β -tubulin heterodimers and are involved in a wide range of cellular functions, including shape maintenance, vesicle transport, cell motility, and division. In the mitotic phase of the cell cycle, microtubules are in dynamic equilibrium with tubulin dimers by assembling the tubulin into microtubules or, conversely, disassembling microtubules to tubulin.¹ Disruption of the dynamic equilibrium can induce cell cycle arrest and ultimately lead to apoptosis. Therefore, the compounds that could inhibit tubulin polymerization or interrupt microtubule depolymerization would be useful in the treatment of cancer. In recent decades several compounds, mostly natural products, targeting tubulin have been discovered and developed; some of them are already in clinical use, such as epothilone, paclitaxel, and vindesine.

On tubulin, the binding sites for paclitaxel, vinblastine, and colchicine are well characterized and distinct.^{2,3} The compounds that bind to vinblastine and colchicine binding sites could inhibit tubulin assembly and are classified as microtubule destabilizing agents. In contrast, the compounds that bind to the paclitaxel binding site prevent microtubule disassembly and are classified as microtubule stabilizing compounds. Although taxanes and vinca alkaloids are effective

antimitotic agents, they have problems with high toxicity, poor bioavailability, synthetic difficulty, and rapid drug resistance. Moreover, the treatment of taxanes and vinca alkaloids induce overexpression of transmembrane efflux proteins that pump the antimitotic inhibitors out of cells. Thus, the dose must be increased to be toxic to tumor cells, resulting in decreased potency and development of multidrug resistance (MDR^a).^{4,5} Because of the undesirable effects discussed above, there is an urgent need to discover new antimitotic agents with better therapeutic properties.

Recent studies reveal that the antitubulin agents targeting the colchicine sites could, in addition to their antimitotic action, shut down the blood supply to tumors by disassembling the microtubules of abnormal vasculatures and changing the endothelial cell morphology, which would consequently cause nutrient starvation of tumor cells and eventually lead to the apoptosis. These vascular-disrupting agents, e.g., combrestatin (CA4), provide a promising new approach in the treatment of cancer and are currently in clinical evaluation for single-drug cancer therapy or multidrug treatment in combination with other cytotoxic drugs and

*To whom correspondence should be addressed. Phone: +886-37-246-166, extension 35713. Fax: +886-37-586-456. E-mail: suying@nhri.org.tw.

^aAbbreviations: MDR, multidrug resistance; CA4, combrestatin; SAR, structure–activity relationship; QSAR, quantitative structure–activity relationship; HY, hydrophobic feature; HYA, hydrophobic aromatic group; HBD, hydrogen bond donor; HBA, hydrogen bond acceptor; EX, excluded volume feature; Hypo1, hypothesis 1; rmsd, root-mean-square deviation; CSIs, colchicine site inhibitors; BrdU, bromodeoxyuridine; SLD, stathmin-like domain; MAP, microtubule-associated protein; DMSO, dimethyl sulfoxide; AUC, area under the curve.

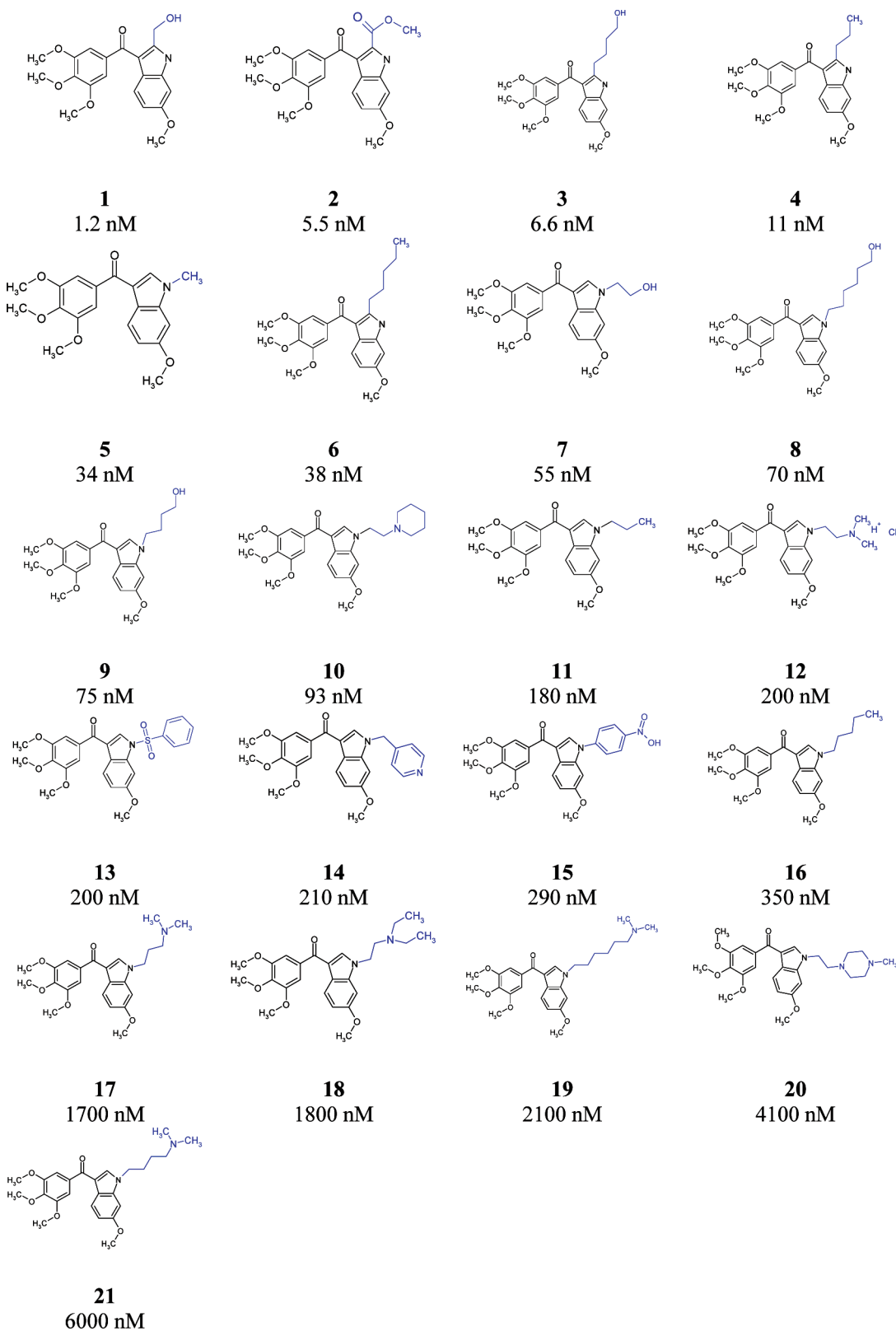


Figure 1. Structures of training-set compounds **1–21** and their experimental IC_{50} values toward KB cell growth.

antiangiogenic agents.⁶ We recently reported the development of an antitubulin agent targeting colchicine binding site, (6-methoxy-1*H*-indol-3-yl)(3,4,5-trimethoxyphenyl)methanone (BPR0L075), which is expected to enter clinical trials next year.⁷ For that program we synthesized several indole-based compounds and evaluated them for anticancer activity, providing us with rich information about the structure–activity

relationship (SAR) in this series of compounds.⁸ In addition to the synthetic program, we have started a computer-aided drug design approach for the development of novel antitubulin agents, which will be the subject of this study.

Virtual screening has emerged as a powerful tool to discover new molecular entities in the treatment of cancer. Depending on the availability of target protein structure, this strategy could

Table 1. Results of Statistical Significance, Correlation Coefficients, and Features of Top-10 Hypotheses^a

hypothesis	correlation	rmsd ^b	total cost	Δ cost ^c	features ^{d,e}					
					HBA	HBD	HY1	HY2	HYA	EX ^f
1	0.963	0.853	84.504	82.279	*	*	*	*	*	2
2	0.923	1.221	92.379	74.404	*	*	*	*	*	2
3	0.920	1.248	93.274	73.509	*	*	*	*	*	1
4	0.909	1.321	95.205	71.578	*	*	*	*	*	1
5	0.906	1.340	95.508	71.275	*	*	*	*	*	
6	0.908	1.332	95.268	71.515	*	*	*	*	*	1
7	0.903	1.364	96.546	70.237	*	*	*	*	*	
8	0.893	1.429	98.351	68.432	*	*	*	*	*	1
9	0.892	1.435	98.405	68.378	*	*	*	*	*	
10	0.885	1.478	99.743	67.04	*	*	*	*	*	

^a Fixed cost of top-10 scoring hypotheses is 76.673. Configuration cost value is 14.5839, and null cost value is 166.783. ^b rmsd, the deviation of log (predicted activities) from the log(experimental activities) normalized by the log(uncertainties). ^c Δ cost = (null cost) – (total cost). ^d HBA, hydrogen bond acceptor; HBD, hydrogen bond donor; HY, hydrophobic group; HYA, hydrophobic aromatic group; EX, number of excluded volumes. ^e The asterisk (*) indicates that these features were present in the hypothesis. ^f Number of excluded volumes of the hypothesis.

Table 2. Experimental and Predicted Activity and Feature Mapping of Training-Set Compounds **1–21** Using the Hypo1 Model

compd	exptl IC ₅₀ (nM)	predicted IC ₅₀ (nM) ^a	error factor ^b	fit value ^c	activity scale ^d	predicted activity scale	mapped features				
							HBA	HBD	HYA	HY1	HY2
1	1.2	0.91	-1.3	10.14	+++	+++	*	*	*	*	*
2	5.5	4.9	-1.1	9.41	+++	+++	*	*	*	*	*
3	6.6	5.4	-1.2	9.37	+++	+++	*	*	*	*	*
4	11	52	+4.5	8.39	+++	+++	*	*	*	*	*
5	34	71	+2.1	8.25	+++	+++	*	*	*	*	*
6	38	42	+1.1	8.48	+++	+++	*	*	*	*	*
7	55	70	+1.3	8.26	+++	+++	*	*	*	*	*
8	70	98	+1.4	8.11	+++	+++	*	*	*	*	*
9	75	65	-1.2	8.29	+++	+++	*	*	*	*	*
10	93	83	-1.1	8.18	+++	+++	*	*	*	*	*
11	180	240	+1.4	7.71	++	++	*	*	*	*	*
12	200	340	+1.7	7.57	++	++	*	*	*	*	*
13	200	70	-2.8	8.25	++	+++	*	*	*	*	*
14	210	300	+1.5	7.62	++	++	*	*	*	*	*
15	290	270	-1.1	7.66	++	++	*	*	*	*	*
16	350	190	-1.8	7.82	++	++	*	*	*	*	*
17	1700	1600	-1.1	6.90	+	+	*	*	*	*	*
18	1800	520	-3.4	7.38	+	++	*	*	*	*	*
19	2100	3300	+1.6	6.58	+	+	*	*	*	*	*
20	4100	3900	-1.1	6.51	+	+	*	*	*	*	*
21	6000	3000	-2	6.62	+	+	*	*	*	*	*

^a The value was estimated by Hypo1. ^b The error factor is calculated as the ratio of the experimental activity to the predicted activity or the inverse if the experimental activity is greater than the predicted activity. ^c Fit value calculated the geometry fitting between the compounds to the hypothesis. ^d Activity scale: highly active, +++, IC₅₀ < 100 nM; moderately active, ++, 100 nM ≤ IC₅₀ < 1000 nM; inactive, +, IC₅₀ ≥ 1000 nM.

be broadly classified into two approaches: structure-based and ligand-based virtual screening. Although the structures of tubulin in complex with various ligands have been determined,⁹ few studies have discussed the discovery of antiproliferative agents by structure-based virtual screening. Kim et al. utilized the tubulin complexed structure to screen a natural product compound database to identify chalcone derivatives as antimiotic agents. The most potent compound showed antiproliferative activity with IC₅₀ of 8.2 μM.¹⁰ Alternatively, several studies have generated pharmacophore models based on the quantitative structure–activity relationship (QSAR) of compounds targeting tubulin and identified the key structural requirements for increasing the activity.^{11–13} None of them, however, further demonstrate the utility of these pharmacophore models to identify new antimiotic agents through virtual screening.

In this study, a ligand-based pharmacophore model was generated on the basis of key chemical features of the indole series of compounds, developed by us, with antiproliferative activity. The pharmacophore model generated was further

characterized and validated by cost analysis and activity prediction ability. Moreover, this model was employed to carry out virtual screening of a chemical database containing approximately 130 000 compounds, which resulted in the identification of four compounds with antiproliferative activity. Most interestingly, one of the compounds, **43**, was identified with potent antiproliferative activity in KB cells with an IC₅₀ of 187 nM. Further biological characterization, including the inhibition of tubulin polymerization and cell cycle arrest in the G₂–M phase, shows that **43** is a novel and potent antimiotic agent with potent antiproliferative activity, which could act as a new lead compound for the development of anticancer therapeutics.

Results and Discussion

Pharmacophore Generation for Tubulin Inhibitors. A training set of 21 indole compounds (**1–21**), with KB cell line inhibition ranging from 1.2 to 6000 nM, was used to generate pharmacophore models by applying the HypoGen module

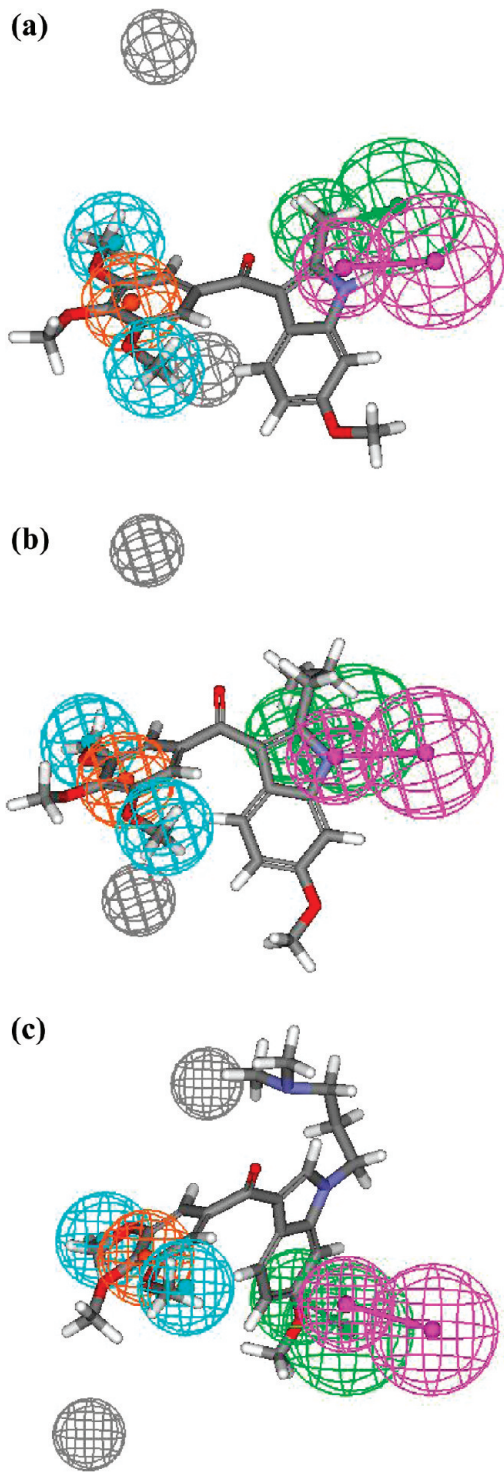


Figure 2. Mapping of training-set compounds **1** (a), **4** (b), and **17** (c) with Hypo1. The magenta spheres represent the HBD, the green spheres represent the HBA, the cyan spheres represent the HY (HY1 and HY2), the dark orange sphere represents the HYA, and the black spheres represent the EX (EX1 and EX2).

of CATALYST (Figure 1). The training-set compounds were selected in such a way to cover over 3 orders of magnitude of activity. This training set contained four compounds already reported by us in the literature and 17 new compounds synthesized in-house.¹⁴ By analysis of the chemical nature of the training-set compounds **1–21**, four features were selected for the pharmacophore model generation, including hydrophobic feature (HY), hydrophobic

Table 3. Validation of the Hypo1 Model Using the CatScramble Program Implemented in Catalyst

validation no. ^a	total cost	fixed cost	rmsd	correlation coefficient	configuration cost
Hypo1	84.5041	76.6728	0.853	0.963196	14.5839
trial 76	86.0934	74.154	1.03317	0.945871	12.0651
trial 93	96.2409	76.6728	1.30717	0.912224	14.5839
trial 95	99.3547	76.4134	1.43792	0.892242	14.3245
trial 1	99.8447	73.9198	1.56524	0.87009	11.8309
trial 36	99.9123	73.8168	1.44859	0.893258	11.7279
trial 25	100.072	73.9198	1.40687	0.901463	11.8309
trial 87	100.195	73.8168	1.56558	0.870285	11.7279
trial 50	100.212	76.6728	1.4882	0.883441	14.5839
trial 84	100.519	73.8168	1.59298	0.865013	11.7279
trial 19	101.897	74.4704	1.60653	0.862667	12.3715

^a The number of top-10 low total cost of the 99 trials generation.

aromatic group (HYA), hydrogen bond donor (HBD), and hydrogen bond acceptor (HBA). Furthermore, to evaluate the steric hindrance that affects the biological activities, the HypoRefine module was utilized to generate excluded volume feature (EX). It represents a spherical point around the ligand binding site that can improve the accuracy of hypothesis to distinguish the inactive agents from the active ones.

By use of these features and passing through constructive, subtractive, and optimization phases, 10 top-ranked hypotheses were generated (Table 1). To further validate the hypotheses generated, cost analysis was applied to reveal the statistical significance of these hypotheses. Two index values were typically used for evaluation: the difference between null cost and fixed cost, and Δ cost (the difference between null and total cost). The fixed cost stands for an ideal hypothesis that perfectly fits the estimated and experimental activities with minimum deviation, while the null cost represents a random hypothesis that cannot predict the activity with respect to the structure. The difference between fixed and null cost should be ≥ 80 bits. The greater the value, the greater the chance of finding useful hypotheses. The difference between the null cost and the fixed cost of the training set was 90.11. In addition, Δ cost for all the 10 hypotheses generated was higher than 60 bits, presenting 90% statistical significance of these models. Hypothesis 1 (Hypo1) was the best pharmacophore model among the 10 hypotheses generated, as characterized by the lowest total cost value (84.504), the greatest cost difference (82.279), the lowest root-mean-square deviation (rmsd) (0.853), and the best correlation coefficient (0.963).

The Hypo1 model consists of two HY, one HBD, one HBA, one HYA, and two EX. Once Hypo1 was identified as the best-ranked model, it was subjected to further evaluation for its predictive ability. The Hypo1 model was utilized to predict the activities of all 21 training compounds (**1–21**). The estimated activities as predicted by Hypo1, the experimental activities, and the corresponding errors (i.e., the ratio of the experimental activity to the predicted activity) are listed in Table 2. It is clear that the IC₅₀ values were well predicted, demonstrating the good predictive quality of Hypo1.

In addition to evaluating the predictive ability of Hypo1, the features of training-set compounds were mapped using Hypo1 (Figure 2). The most active compound, **1**, mapped well to all the features of Hypo1 (Figure 2a and Table 2): the phenyl rings mapped on HYA feature; two methoxyl groups overlapped with the HY features; and the nitrogen atom of

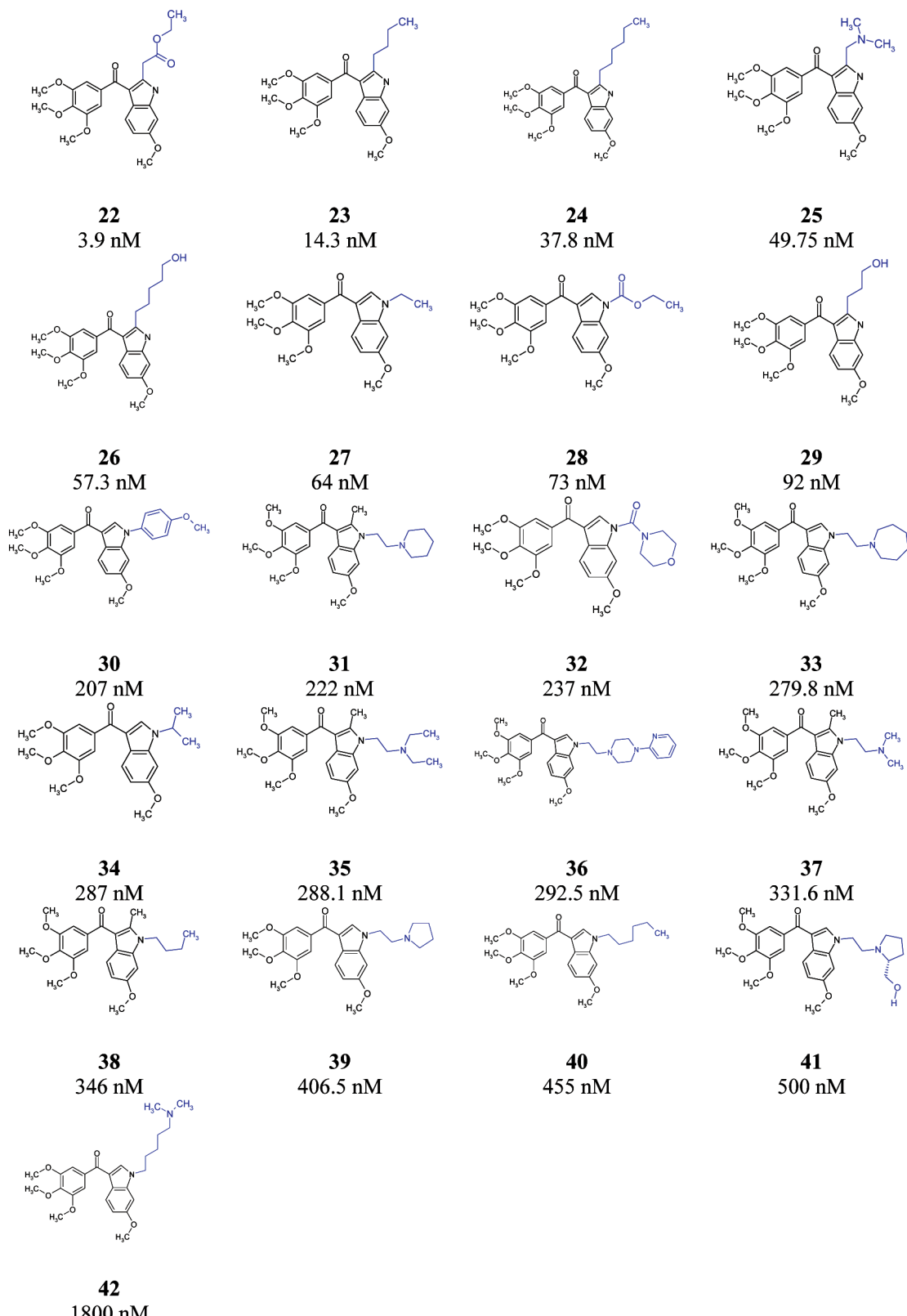


Figure 3. Structures of testing-set compounds **22–42** and their experimental IC_{50} values toward KB cell growth.

indole served as HBD. Moreover, the HBA is close to the oxygen atom of the hydroxyl function group. To further investigate compounds with lower activity in the training set, the moderately active compound **4** (Figure 2b) and inactive compound **17** (Figure 2c) were mapped on Hypo1. The mapping revealed that compounds **4** and **17** missed HBA and HBD features, respectively (Table 2). As

can be seen from Table 2, the mapped features in weak inhibitors missed one or two critical features, such as HBA and HBD. In general, compounds with lower activity did not map on the HBD feature of Hypo1, but compounds with higher activity all kept the HBD feature, demonstrating the importance of this feature for maintaining high potency.

Table 4. Experimental and Predicted Activity and Feature Mapping of Testing-Set Compounds 22–42 Using the Hypo1 Model^a

compd	true IC ₅₀ (nM)	estimated IC ₅₀ (nM)	error factor ^b	activity scale ^c	estimated activity scale	mapping features ^{d,e}				
						HBA	HBD	HYA	HY1	HY2
22	3.9	1.9	-2	+++	+++	*	*	*	*	*
23	14.3	37	2.6	+++	+++	*	*	*	*	*
24	37.8	36	-1.1	+++	+++	*	*	*	*	*
25	49.75	40	-1.3	+++	+++	*	*	*	*	*
26	57.3	77	1.4	+++	+++	*	*	*	*	*
27	64	92	1.4	+++	+++	*	*	*	*	*
28	73	41	-1.8	+++	+++	*	*	*	*	*
29	92	68	-1.4	+++	+++	*	*	*	*	*
30	207	210	1	++	++	*	*	*	*	*
31	222	130	-1.8	++	++	*	*	*	*	*
32	237	140	-1.6	++	++	*	*	*	*	*
33	279.8	170	-1.7	++	++	*	*	*	*	*
34	287	160	-1.8	++	++	*	*	*	*	*
35	288.1	81	-3.5	++	+++	*	*	*	*	*
36	292.5	660	2.2	++	++	*	*	*	*	*
37	331.6	100	-3.3	++	++	*	*	*	*	*
38	346	120	-2.9	++	++	*	*	*	*	*
39	406.5	490	1.2	++	++	*	*	*	*	*
40	455	880	1.9	++	++	*	*	*	*	*
41	500	160	-3.1	++	++	*	*	*	*	*
42	1800	1900	1	+	+	*	*	*	*	*

^aThe correlation coefficient is 0.89. ^bThe error factor is calculated as the ratio of the experimental activity to the predicted activity or the inverse if the experimental activity is greater than the predicted activity. ^cActivity scale: highly active, +++, IC₅₀ < 100 nM; moderately active, ++, 100 nM ≤ IC₅₀ < 1000 nM; inactive, +, IC₅₀ ≥ 1000 nM. ^dHBA, hydrogen bond acceptor; HBD, hydrogen bond donor; HY, hydrophobic group; HYA, hydrophobic aromatic group. ^eThe asterisk (*) indicates that the feature was consistent with the hypothesis.

Validation of the Hypo1 Model. The CatScramble module in CATALYST was used to further validate the statistical relevance of the Hypo1 pharmacophore model by the principle of Fisher's randomization test. Random hypotheses were generated by randomly reassigning the activity to all compounds in the training set (**1–21**) and consequently using the same features and parameters of Hypo1 to construct the models. If the random hypotheses have higher total cost, rmsd, and lower correlation coefficient, the original hypothesis, Hypo1, would be regarded as statistically significant rather than generated by chance. To reach a 99% confidence level, 99 random hypotheses (random spreadsheets) must be generated (significance = [1 – (1 + 0)/(99 + 1)] × 100% = 99%). As listed in Table 3, the statistics of Hypo1 are better than other random hypotheses, as revealed by the lowest total cost, lowest rmsd, and highest correlation coefficient, which verify that the Hypo1 hypothesis was not obtained by chance.

To further validate the Hypo1 model, it was assessed by its predictive capability on a testing-set of 21 new compounds, **22–42** (Figure 3). All the testing-set compounds activities were predicted correctly (Table 4); moreover, the correlation coefficient for the testing-set compounds given by Hypo1 is 0.89. These demonstrate the predictive accuracy of the Hypo1 model. All of the testing-set compounds mapped two HY and one HYA. The most active compound has additional HBD and HBA features. Modest inhibitors have only one additional HBD feature, while the weak inhibitors have only one additional HBA feature, which is consistent with the observation in the training-set compound where the HBD and HBA features, particularly the HBD feature, are important for maintaining high potency in this series of compounds.

Virtual Screening Using the Hypo1 Model. Since this study aims not only to generate the pharmacophore model to gain insight into the important features responsible for inhibition

and predict compound activities but also to search for novel inhibitors by virtual screening using the constructed pharmacophore model, we further employed the Hypo1 model to screen the ChemDiv database and an in-house compound collection consisting of around 130 000 compounds. The top 1000 compounds fulfilling all the features described by Hypo1 and predicted as highly active compounds were subjected to further analysis. Visual inspection of all of them to rule out those compounds that might clash with the tubulin binding site led to the selection of 142 compounds. The above selected 142 compounds were then experimentally evaluated for their antiproliferative activities against the human oral squamous carcinoma KB cell line. Out of these, four compounds, **43–46**, showed KB cell line inhibition with IC₅₀ < 10 μM and were selected for further analyses. Compounds **43**, **44**, **45**, and **46** showed inhibition with IC₅₀ of 0.187, 2.0, 3.0, and 5.7 μM, respectively.

Once **43–46** were identified as antiproliferative agents, the features of these compounds were mapped using Hypo1 to get insight into the molecular feature enabling them for antiproliferative activity and are depicted in Figure 4. For the most potent compound, **43**, the HYA was mapped onto the benzene ring, and the HY was located with the two chlorine atoms. These are known crucial features for the activity of inhibitors against tubulin as reported previously^{15,16} and also found in this study. The HBA feature was mapped onto the oxygen atom of the carbonyl group, and the HBD feature was mapped on the nitrogen atom of the amide group. The features of EX were correctly located because no atoms were fitted near those spheres.

Biological Activity of 43. Because of the chemical novelty and the high activity against the human cancer KB cell line of **43**, we explored the potential of this compound using various biological assays. Thus, in addition to the KB cell line, further studies showed **43** inhibited the proliferation of various other cancer cells growth, including MCF-7,

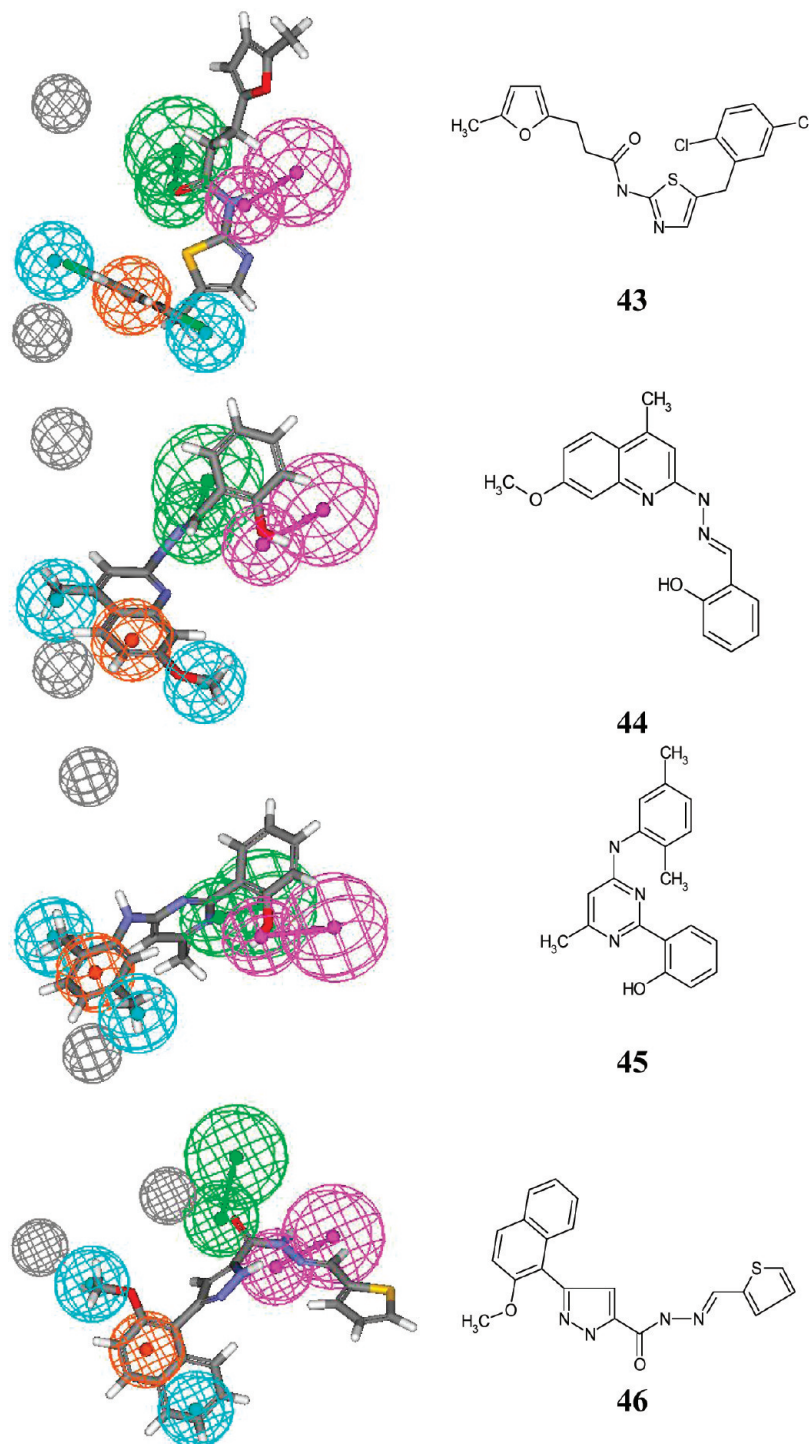


Figure 4. Structures of four hit compounds **43–46** identified via pharmacophore-based virtual screening and their corresponding mapping with Hypo1. The magenta spheres represent the HBD, the green spheres represent the HBA, the cyan spheres represent the HY (HY1 and HY2), the dark-orange sphere represents the HYA, and the black spheres represent the EX (EX1 and EX2).

NCI-H460, and SF-268 (Table 5). Among the tested cancer cells, **43** exhibited the strongest inhibition to the proliferation of KB cells, with an IC_{50} of 187 nM.

To understand the effect of **43** on cell-cycle progression and to delineate the mechanism of action for the high antiproliferative activity, cell cycle analysis using flow cytometry was carried out. Various concentrations of **43** were incubated with KB cells for 24 h, and the cells were analyzed. Cell cycle analysis results showed that **43** caused accumulation of KB cells in the G₂-M phase with concurrent loss of the

G₀-G₁ phase in a dose dependent manner (Figure 5a). When treated with 400 nM **43**, the cells started to show substantial accumulation in the G₂-M phase (55.6%). Further increasing the concentration of **43** to 800 nM resulted in the arrest of 70.3% KB cells in the G₂-M phase, showing that the compound blocks the mitotic phase of the cell cycle. Moreover, further cell cycle study revealed that treatment with **43** resulted in the accumulation of KB cells in the G₂-M phase with concomitant decrease of the G₀-G₁ phase in a time dependent manner. As shown in Figure 5b, the cells

started to significantly accumulate in the G₂-M phase after 8 h of treatment with **43** and reached a maximum accumulation by 16 h. However, the sub-G₁ phase (a hypodiploid DNA content peak indicated apoptotic cells) started to show substantial accumulation after 24 h and increased with time. The accumulation of cells in the G₂-M phase initially followed by the increase of the sub-G₁ phase with simultaneous decrease of the G₂-M phase at later time points confirmed **43** induced G₂-M arrest before the cells went into apoptosis.

Furthermore, the training-set compounds act as tubulin polymerization inhibitors by binding to the colchicine site of tubulin.⁷ Therefore, it is reasonable to assume that the hypotheses generated from the structures of training-set compounds represent the binding mode of colchicine site

Table 5. Antiproliferative activities of **43** against various cancer cell lines (IC_{50} , nM)^a

compd	KB ^b	MCF-7 ^c	NCI-H460 ^d	SF-268 ^e
43	187	236	285	319

^a IC_{50} value is the concentration of test compound required to inhibit cell growth. ^b KB, human oral squamous carcinoma. ^c MCF-7, breast cancer cell line. ^d NCI-H460, human non-small-cell lung cancer cell line. ^e SF-268, human central nervous system cancer cell line.

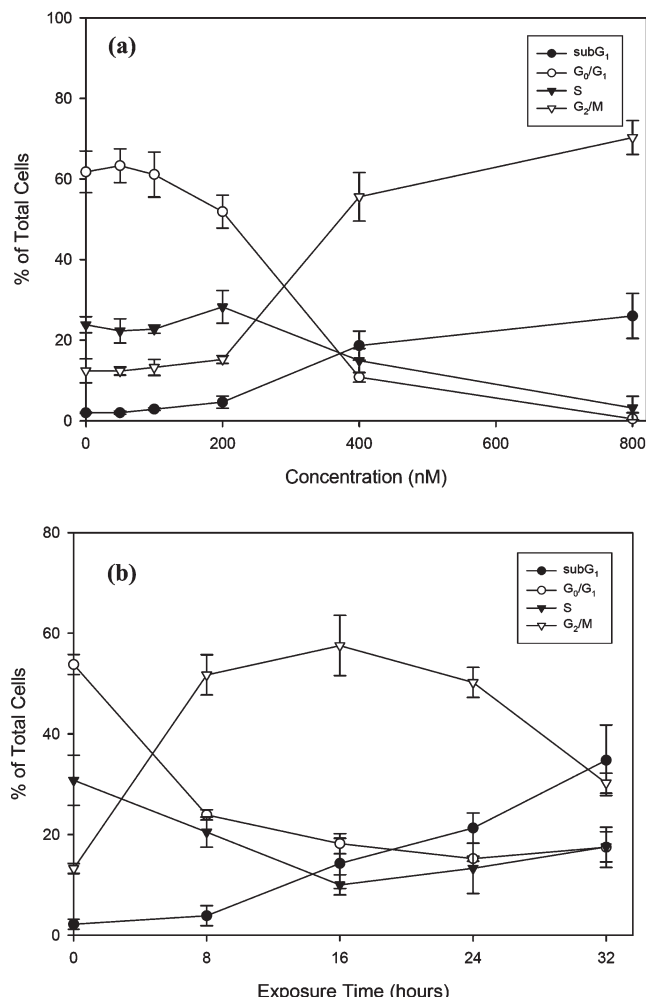


Figure 5. Dose and time effect of **43** on cell cycle distribution in KB cells. (a) Cells were treated with various concentrations of **43** for 24 h. (b) Cells were incubated with 400 nM **43** for the indicated times and analyzed for propidium iodide-stained DNA content by flow cytometry.

inhibitors (CSIs) with the tubulin and it is logical to expect the virtual screening using the Hypo1 model to identify colchicine site binding agents with antitubulin activity.

Hence, to examine whether **43** is a tubulin inhibitor, an *in vitro* tubulin polymerization assay was performed. Various concentrations of **43** were incubated with unpolymerized microtubule-associated protein-rich tubulin, and the absorbance at 350 nm was measured to show the effect of the compound on tubulin polymerization (Figure 6). In the absence of test compound as a control experiment, absorbance at 350 nm increased with time. In the presence of **43**, tubulin polymerization was inhibited in a dose-dependent manner, as measured by the absorbance at 350 nm. The novel inhibitor **43** identified through virtual screening in the present study showed inhibition of tubulin polymerization with an IC_{50} of 4.4 μ M. It is interesting to note that the tubulin polymerization inhibition potency ($IC_{50} = 4.4 \mu$ M) of **43** is weaker than its antiproliferative potency ($IC_{50} = 187$ nM). Indeed, the weaker tubulin polymerization inhibition compared with the antiproliferative potency is commonly observed in many tubulin inhibitors. For example, the IC_{50} values of a 3-aryllindole analogue, a potent tubulin inhibitor resembling the combretastatin-4 structure, in inhibiting of tubulin polymerization and cell proliferation growth are around 2.18 μ M and 1 nM, respectively.⁸ An oxadiazoline, discovered by Abbott as a potent tubulin inhibitor, inhibited the tubulin polymerization with an IC_{50} value of 4.5 μ M, while it showed the inhibition of the cancer cell line with an IC_{50} value of 42.2 nM.¹⁷ Chalcone, another class of tubulin inhibitor, showed tubulin polymerization inhibition with an IC_{50} value of 10 μ M, while it demonstrated strong inhibition against cell proliferation with an IC_{50} value of 10 nM.¹⁸ In addition, indanocine, a tubulin inhibitor discovered by the University of California, inhibited tubulin polymerization and cell growth with an IC_{50} of 1.7 μ M and 1 nM, respectively.¹⁹ More examples could be found in various publications.^{20–22} As could be seen, many of the tubulin inhibitors showed much stronger antiproliferative potency in the cell than in the *in vitro* tubulin polymerization inhibition, which is consistent with the observation of **43**. The reason that the antiproliferative potency of tubulin inhibitors is higher than its tubulin inhibition potency might be due to the fact that tubulin polymerization assay is less sensitive than the cell antiproliferation assay, and therefore, higher concentrations of test compounds, usually in the micromolar range, were required to show tubulin inhibition effects. Additionally, these two assays had different experimental design, conditions, and influence factors, which would result in the difference in the IC_{50} values.

Finally, the tumor histoculture system was employed to evaluate the anticancer activity of **43**. The histoculture is an *in vivo*-like three-dimensional culture system, and the result of the histoculture model has been shown to correlate to the clinical outcome in several carcinomas.^{23,24} The representative tissue sections of the histocultures of human colorectal HCT116 xenograft tumors with and without treatment of **43** are shown in Figure 7. In the control experiment, the proliferating tumor cells were immunostained for the DNA-incorporated bromodeoxyuridine (BrdU) in brown and the nonproliferating tumor cells were counterstained with hematoxylin in blue (Figure 7a). When the tumors were treated with 1 μ M **43**, more cells became blue, indicated as nonproliferating tumor cells (Figure 7b). On increasing the concentration of **43** to 10 μ M, a greater number of blue-stained cells were

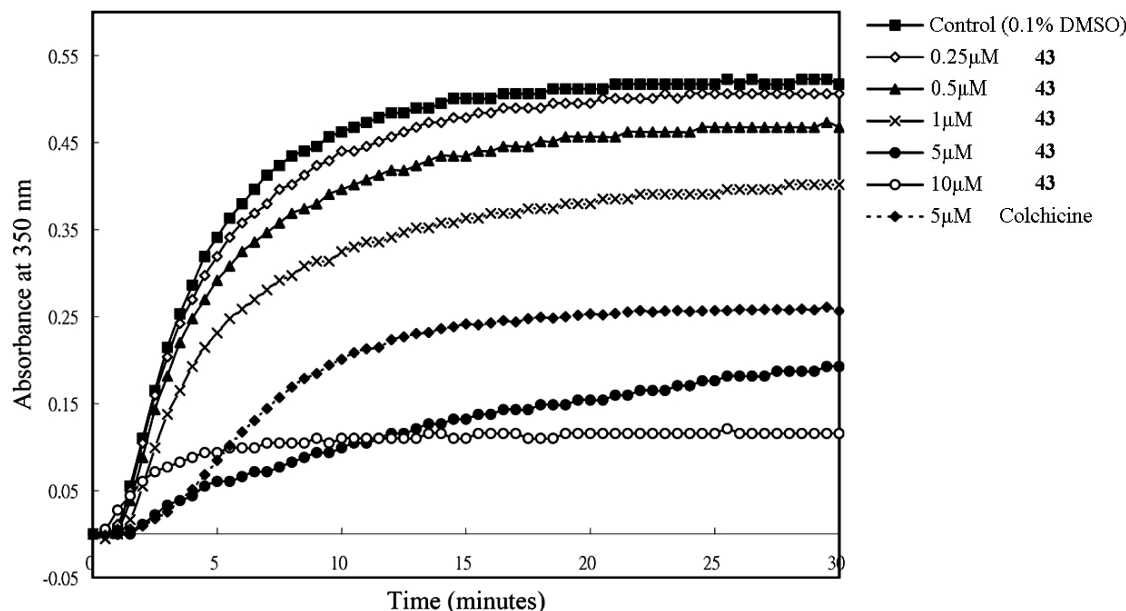


Figure 6. In vitro tubulin polymerization assay. Purified tubulin in a reaction buffer was incubated in the absence (control, ■) or the presence of colchicine (5 μM, □) or **43** (0.25 μM, △; 0.5 μM, ▲; 1 μM, ×; 5 μM, ●; 10 μM, ○). **43** inhibited tubulin polymerization in a dose dependent manner with an IC₅₀ of 4.4 μM.

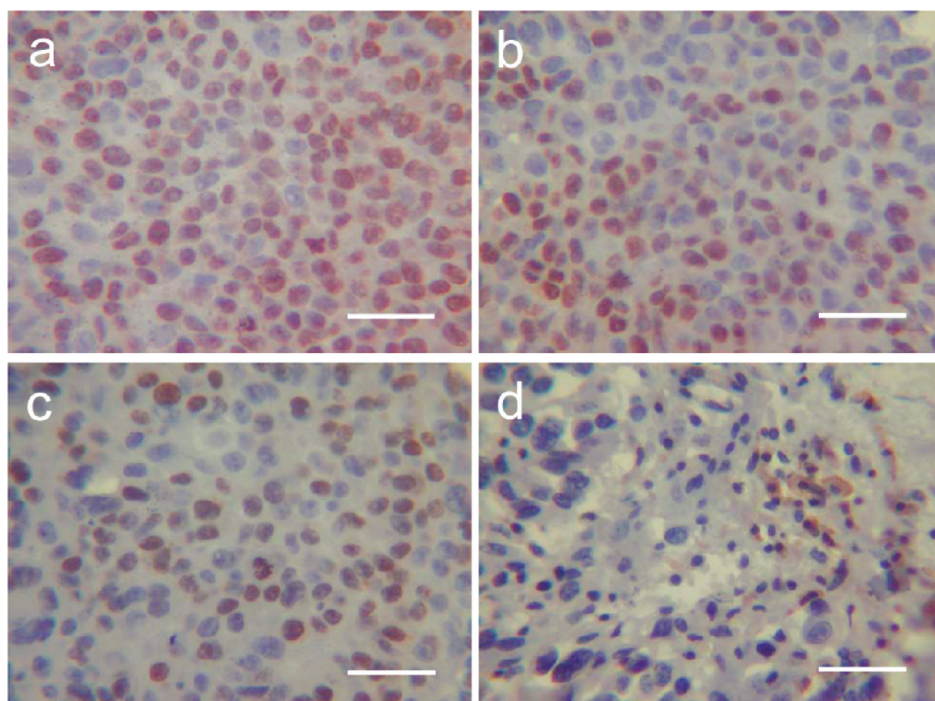


Figure 7. Illustrations of immunostaining of human colorectal HCT116 xenograft tumors without and with treatment of **43**. Proliferating tumor cells were BrdU-incorporated in brown shown (a) treated with the vehicle culture medium, (b) treated with 1 μM **43**, (c) treated with 10 μM **43**, and (d) treated with 100 μM **43**. Each scale bar is 50 μm.

observed (Figure 7c). Up to 100 μM, almost all cells were stained in blue (Figure 7d). These results demonstrate anti-proliferation activity of **43** in a concentration-dependent manner in an in vivo-like histoculture system.

Mapping of Hypo1 onto the Colchicine-Binding Site and Molecular Modeling of **43.** Since the Hypo1 model was generated from a set of CSIs and this pharmacophore model was assumed to represent the binding mode of CSIs on tubulin, it would be interesting to know if Hypo1 indeed maps well onto the published colchicine-binding site of tubulin. Hence, to further investigate the relationship of

Hypo1 with the colchicine-binding site, Hypo1 was mapped onto the colchicine-binding site of tubulin. As shown in Figure 8, Hypo1 consisted of one HBD, one HBA, two HY (HY1 and HY2), one HYA, and two EX (EX1 and EX2). The HY1, HY2, and HYA are located in the hydrophobic region of the colchicine-binding site. Several residues in the hydrophobic region, including Leu242, Leu248, Ala250, Leu255, and Ala316 region, were close to the HY1, HY2, and HYA. The HBD of Hypo1 was directed to Thr179 of the colchicine-binding site, and the HBA feature pointed to the side chain of Asn101 that served as the

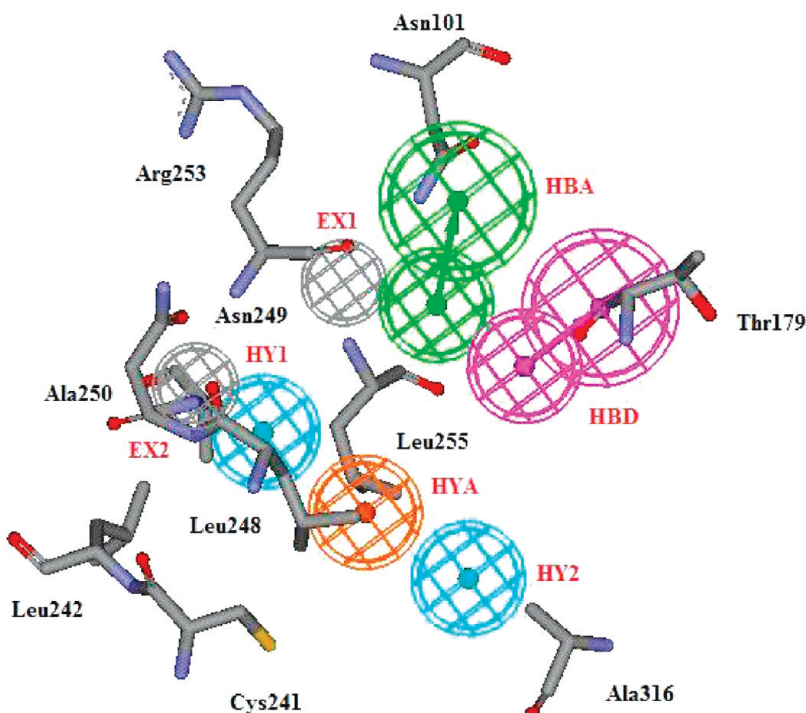


Figure 8. Mapping of Hypo1 with the residues of colchicine-binding site. The features of Hypo1 were complementary to the colchicine site on tubulin. The HY feature (shown in cyan) and the HYA feature (shown in dark orange) are close to Leu242, Leu248, Ala250, Leu255, and Ala316. The HBD feature (shown in magenta) pointed to Thr179, and the HBA feature (shown in green) was directed to Asn101.

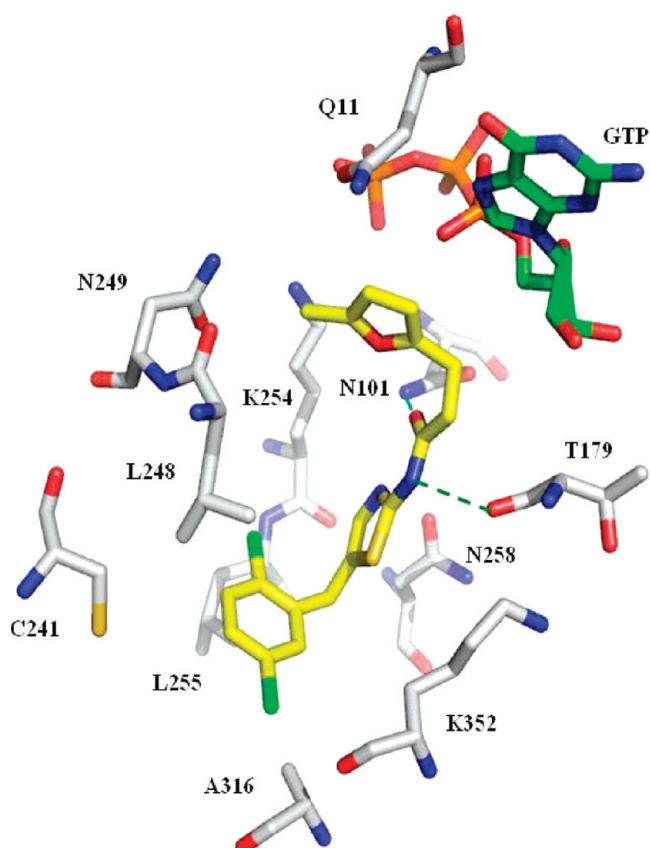


Figure 9. Docking position of **43** (yellow) in the colchicine-binding site of tubulin. The green lines are the potential H-bond between Thr179, Asn101 and **43**, and the distances are 2.89 and 3.05 Å, respectively.

hydrogen donor. Finally, the two excluded volumes, EX1 and EX2, were located at the main chain positions of Arg253

and Asn249, respectively, indicating the restriction of CSI at these positions.

To further elucidate the interactions of newly identified **43** with tubulin, a molecular modeling study was carried out. **43** was docked into the colchicine-binding site of tubulin by the program GOLD, version 3.2 (CCDC Software Limited, Cambridge, U.K.). The crystal structure of tubulin in complex with colchicine (PDB code 1SA0)⁹ was used as the template, and the region within a radius of 20 Å centered on the CD2 atom of Leu248 was defined as the binding site for the docking study. The docking study revealed **43** bound to the colchicine-binding site via two hydrogen bonds with Thr179 and Asn101, with distances of 2.89 and 3.05 Å, respectively (Figure 9). The N atom of the side chain in Asn101 served as hydrogen bond donor to the carbonyl group on **43**, and the oxygen of main chain of Thr179 formed the H bond with the N atom of the amide linker between the furan and thiazole rings. In addition, the dichlorobenzyl group and thiazol ring of **43** made hydrophobic interactions with Leu248, Leu255, Ala316, and Asn258. Finally, the 5-methylfuran group of **43** had close contacts with Asn249, Lys254, and Gln11.

It is interesting to note that there are two published conformations for the tubulin structure. One is the straight conformation,²⁵ and the other is the curved conformation capped⁹ by the stathmin-like domain (SLD) of RB3 (one of the member of stathmin-like family). The SLD of RB3 bends the tubulin tetramer (four subunits) and increases the distance between the α subunit and β subunit, which consequently opened up the interface of the α subunit and the β subunit to make more space for the binding of colchicine to the intermediate domain of the β subunit. Comparing these two conformations showed differences in the colchicine binding site. The T7 loop and the H8 helix shifted in the tubulin–colchicine complex to allow the accommodation of

colchicine in the curved conformation, whereas the straight conformation has limited space for the colchicine binding. Although the curved structure is used as the template for the Hypo1 mapping and docking study presented in this paper, as it is the available structure solved in complex with colchicine, we could not rule out the possibility of the Hypo1, and our compound, **43**, could also map/bind to the straight conformation and has different spatial arrangement from the current docking study. Definitely, additional information is required to validate our mapping and docking study. Particularly, the availability of protein structure of straight tubulin in complex with colchicine would provide more insights on the mapping of Hypo1 and docking of **43** on the colchicine binding site.

Conclusion

In this study, we present a successful example of employing pharmacophore-based virtual screening to identify novel compounds with antiproliferative activity through their ability to inhibit tubulin polymerization. Initially, a pharmacophore model, Hypo1, was built on the basis of 21 training-set indole compounds possessing varying levels of antiproliferative activity and then was subjected to careful validation. The Hypo1 pharmacophore model possessed one HBD, one HBA, two HY (HY1 and HY2), one HYA, and two EX (EX1 and EX2). These features identified by the Hypo1 model truly reflected the features of tubulin inhibitors and are crucial for the binding of CSIs to the colchicine-binding site in tubulin. Moreover, Hypo1 demonstrated a high degree of reliability in its predictive ability, as judged by the high correlation coefficient values between the experimental data and predicted activities of both training-set and test-set compounds. Therefore, the Hypo1 pharmacophore model could not only provide rationales for further lead optimization but also be applied to estimate the activity of newly designed compounds so that the compounds with higher predicted activity could be prioritized for synthesis.

Further, utilization of the Hypo1 pharmacophore model to screen chemical database in silico led to the identification of four compounds with antiproliferative activity. Among these, **43** showed potent antiproliferative activity against various cancer cell lines, with IC₅₀ values in the nanomolar range. Among the tested cancer cells, **43** exhibited the strongest inhibition on the proliferation of KB cells with an IC₅₀ of 187 nM. Further biological characterization revealed that **43** effectively inhibited tubulin polymerization and significantly induced cell cycle arrest in G₂-M phase. **43** also demonstrated the in vivo-like anticancer effects using the histoculture system. To our knowledge, **43** is the most potent antiproliferative compound with antitubulin activity discovered by computer-aided drug design. It is interesting to note that the newly identified compound **43** already possesses low nanomolar level antiproliferative activity without any chemical synthesis efforts involved. Moreover, as most of the studies are devoted to develop analogues of colchicine and CA4 as tubulin inhibitors, the chemical structure of **43** is distinct from these agents and could serve as a novel hit worthy of lead optimization efforts. In addition, all the compounds used to construct the Hypo1 model contained the trimethoxyphenyl moiety, but our hits, interestingly, did not have this moiety. Many tubulin inhibitors have been found with the trimethoxyphenyl moiety, and this moiety has been reported as an important pharmacophore for inhibition to tubulin. For example, colchicine

contained the trimethoxy group and the replacement of the methyl group with bulky groups resulted in substantial loss of the activity.²⁶ In the 3-aryllindole series, potent antitubulin agents reported by Hsieh's laboratory also had the trimethoxyphenyl group. SAR studies of the 3-aryllindole series revealed that removal of all three methoxyl groups or the methoxyl group at the C5 position abolished the activity.⁸ Cushman et al. reported that the removal of either the C-4 or the C-5 methoxy group on the phenyl ring causes a substantial loss of activity in the stilbene analogues.²⁷ Other structurally diverse tubulin inhibitors have been reported to contain the trimethoxyphenyl moiety, and the importance of this particular moiety was discussed in various publication.^{28,29} Interestingly, our hit, **43**, did not contain the trimethoxyphenyl moiety but showed potency in the cytotoxicity activity, tubulin polymerization inhibition, and xenograft experiments. Comparison of the docking structure of **43** with the structure of tubulin in complex with colchicine⁹ revealed that the 2, 5-dichlorobenzyl group of **43** and the trimethoxyphenyl group of colchicine occupied a similar region in the tubulin and both had interactions with the surrounding residues, for example, Leu248, Leu255, and Ala316. Moreover, mapping of **43** and **1** into Hypo1 revealed that the 2,5-dichlorobenzyl group of **43** and the trimethoxyphenyl group of **1** occupied the same pharmacophore features, HY and HYA. All of these results indicated that the dichlorobenzyl group of **43** might share similar interactions and functions with the trimethoxyphenyl group in the known tubulin inhibitors. Future work on the lead optimization and SAR studies of **43** would provide more insights on the role of the dichlorobenzyl group.

Experimental Section

Growth Inhibition Assay. The assay was performed as reported earlier.³⁰ Briefly, cells at a density of 5000 (cells/mL)/well were seeded into 24-well plates and for 24 h for attachment. The cells were incubated with various concentrations of test drugs for three generations. Then methylene blue dye was added to evaluate the effect of compounds on cell growth. The 50% inhibition of cell growth value (IC₅₀) was calculated as a comparison with untreated cells (taken as 100%).

MTS Assay. MTS assay was also performed in determining the growth inhibition of cancer cells. Briefly, MCF-7, NCI-H460, and SF-268 cells were seeded into 96-well plates at 6500, 2500, and 7500 cells/well, respectively. After 24 h for attachment, test compound was added into each well and incubated for three generations. After removal of the supernatant, a total of 100 μ L of MTS reaction reagent containing the medium, MTS, and PMS (Promega, Madison, WI) in a ratio of 8:2:0.1, respectively, was added into each well to react with dehydrogenase enzyme in survival cells. After 1.5 h, the absorbance at 490 nm was monitored using a PerkinElmer Victor2 plate reader (PerkinElmer, Shelton, CT).

Cell Cycle Analysis. DNA flow cytometry was used to monitor the cell cycle progression. Exponentially growing human oral squamous carcinoma cells (KB) were incubated with various concentrations of compounds for 24 h. Following treatment with test compound, cells were trypsinized, then washed with PBS and fixed in 80% ethanol at -20 °C for 1 h. The 50 μ g/mL propidium iodide and 50 μ g/mL RNase were used to stain the fixed cells in the dark for 20 min at room temperature. The DNA content was analyzed using a fluorescence-activated cell sorting iv flow cytometer (BD Biosciences, Franklin Lakes, NJ). A total of 10 000 cells were counted at each analysis, and the percentage of cells in each phase was calculated using the ModFit LT software (Verity Software House, Topsham, ME).

In Vitro Microtubule Assembly Assay. The assay was performed in a 96-well plate, as described previously.³¹ Briefly, microtubule-associated protein-rich (MAP-rich) tubulin in 100 μ L of buffer containing 100 mM PIPES (pH 6.9), 1 mM GTP, 2 mM MgCl₂, and 2% (v/v) dimethyl sulfoxide (DMSO) was mixed with various concentrations of test compound in 96-well plates. The increase in absorbance was monitored at 350 nm in a PowerWave X microplate reader (BIO-TEK Instruments, Winooski, VT) and recorded every 30 s for a total of 30 min at 37 °C. The concentration that inhibited tubulin polymerization by 50% (IC₅₀) was determined by the area under the curve (AUC). The 100% polymerization was defined as the AUC of the untreated control, and the IC₅₀ was calculated by nonlinear regression.

Measurement of Cell Proliferation. As reported previously,³² the histocultures were incubated with 40 μ M BrdU for 48 h after compound treatments, washed with PBS, fixed in 3.7% neutralized formalin, dehydrated in ethanol solutions, and then embedded in paraffin. Proliferating tumor cells incorporating BrdU molecules were detected using the BrdU antibody M744 visualized in brown. Tissue sections were counterstained with Mayer's hematoxylin from Shandon (Pittsburgh, PA), and nonproliferating cells were stained in blue nuclei.

Pharmacophore Generation with CATALYST. The two-dimensional structures of the compounds were sketched and converted to 3D structures using Visualizer module in CATALYST 4.10 (Accelrys Inc. (www.accelrys.com)). The best conformer generation method (20 kcal/mol energy threshold; the maximum number of conformers is 250) was used, which involved applying a poling algorithm to obtain more complete coverage of a chemical's conformational extent and reduce conformational redundancies. Conformations were minimized to local minimum conformers with the CHARMM force field. To conduct a predictive model, the HypoGen module was employed and four features were selected (hydrophobic, hydrophobic aromatic, hydrogen donor, and acceptor). Default parameters were used except for the uncertainty value, which was set at 2.0 to take into account the biological data. In addition, the HypoRefine algorithm was used to include the excluded volumes which can predict compounds with poor activity due to the steric effect.

Database Preparation and Searching. The 2D structures of the compound database (ChemDiv Inc. (www.chemdiv.com)) were converted to 3D SD format by DBconvert module in Insight II. Each compound generated multiconformers by a fast conformer generation method in CATALYST 4.10, and then they were combined for visual screening. Library Screen module in CATALYST 4.10 was performed to select the candidates, with the number of minimum and maximum features both being 5. Using the BEST flexible search method to modify the conformations of compounds during execution time can provide a more accurate search and increase the number of hits.

Docking Study. The GOLD program, version 3.2 (CCDC Software Limited, Cambridge, U.K.) was applied to perform the molecular modeling study of **43** into the colchicine binding site of tubulin. The X-ray structure of tubulin in complex with colchicine was used as the template (PDB code 1SA0),⁹ and the region within a radius of 20 Å centered on the CD2 atom of Leu248 was defined as the binding site for the docking study. Twenty genetic algorithm (GA) runs were performed for **43** docking. For each GA run, 100 000 operations were carried out with a population size of 100 on a set of five islands. The weights for three types of operations (crossover, mutation, and migration) were set as the default values. The selection pressure, which is the ratio of the probability of the most fit member selected as a parent to the probability of an average member selected as a parent, was set to 1.1. The annealing parameters of 4.0 and 2.5 Å for van der Waals and hydrogen bonding were applied to allow poor geometry at the beginning of a GA run. The scoring function, GoldScore, implemented in the GOLD program was chosen to rank the docking poses of **43**.

Acknowledgment. We thank Hsiao-Wen Edith Chu, Tai-Tsung Chen, and Hsiu-Hsiu Huang for their administrative support, we thank the National Health Research Institutes for financial support.

References

- Valiron, O.; Caudron, N.; Job, D. Microtubule dynamics. *Cell. Mol. Life Sci.* **2001**, *58*, 2069–2084.
- Sengupta, S.; Thomas, S. A. Drug target interaction of tubulin-binding drugs in cancer therapy. *Expert Rev. Anticancer Ther.* **2006**, *6*, 1433–1447.
- Carlson, R. O. New tubulin targeting agents currently in clinical development. *Expert Opin. Invest. Drugs* **2008**, *17*, 707–722.
- Dumontet, C.; Sikic, B. I. Mechanisms of action of and resistance to antitubulin agents: microtubule dynamics, drug transport, and cell death. *J. Clin. Oncol.* **1999**, *17*, 1061–1070.
- Zhang, Q.; Peng, Y.; Wang, X. I.; Keenan, S. M.; Arora, S.; Welsh, W. J. Highly potent triazole-based tubulin polymerization inhibitors. *J. Med. Chem.* **2007**, *50*, 749–754.
- Hsieh, H. P.; Liou, J. P.; Mahindroo, N. Pharmaceutical design of antimitotic agents based on combretastatins. *Curr. Pharm. Des.* **2005**, *11*, 1655–1677.
- Kuo, C. C.; Hsieh, H. P.; Pan, W. Y.; Chen, C. P.; Liou, J. P.; Lee, S. J.; Chang, Y. L.; Chen, L. T.; Chen, C. T.; Chang, J. Y. BPROL075, a novel synthetic indole compound with antimitotic activity in human cancer cells, exerts effective antitumoral activity in vivo. *Cancer Res.* **2004**, *64*, 4621–4628.
- Liou, J. P.; Chang, Y. L.; Kuo, F. M.; Chang, C. W.; Tseng, H. Y.; Wang, C. C.; Yang, Y. N.; Chang, J. Y.; Lee, S. J.; Hsieh, H. P. Concise synthesis and structure–activity relationships of combretastatin A-4 analogues, 1-aryloylindoles and 3-aryloylindoles, as novel classes of potent antitubulin agents. *J. Med. Chem.* **2004**, *47*, 4247–4257.
- Ravelli, R. B.; Gigant, B.; Curmi, P. A.; Jourdain, I.; Lachkar, S.; Sobel, A.; Knossow, M. Insight into tubulin regulation from a complex with colchicine and a stathmin-like domain. *Nature* **2004**, *428*, 198–202.
- Kim do, Y.; Kim, K. H.; Kim, N. D.; Lee, K. Y.; Han, C. K.; Yoon, J. H.; Moon, S. K.; Lee, S. S.; Seong, B. L. Design and biological evaluation of novel tubulin inhibitors as antimitotic agents using a pharmacophore binding model with tubulin. *J. Med. Chem.* **2006**, *49*, 5664–5670.
- Zhang, S. X.; Feng, J.; Kuo, S. C.; Brossi, A.; Hamel, E.; Tropsha, A.; Lee, K. H. Antitumor agents. 199. Three-dimensional quantitative structure–activity relationship study of the colchicine binding site ligands using comparative molecular field analysis. *J. Med. Chem.* **2000**, *43*, 167–176.
- Ducki, S.; Mackenzie, G.; Lawrence, N. J.; Snyder, J. P. Quantitative structure–activity relationship (5D-QSAR) study of combretastatin-like analogues as inhibitors of tubulin assembly. *J. Med. Chem.* **2005**, *48*, 457–465.
- Tripathi, A.; Fornabaio, M.; Kellogg, G. E.; Gupton, J. T.; Gewirtz, D. A.; Yeudall, W. A.; Vega, N. E.; Mooberry, S. L. Docking and hydropathic scoring of polysubstituted pyrrole compounds with antitubulin activity. *Bioorg. Med. Chem.* **2008**, *16*, 2235–2242.
- Liou, J. P.; Mahindroo, N.; Chang, C. W.; Guo, F. M.; Lee, S. W.; Tan, U. K.; Yeh, T. K.; Kuo, C. C.; Chang, Y. W.; Lu, P. H.; Tung, Y. S.; Lin, K. T.; Chang, J. Y.; Hsieh, H. P. Structure–activity relationship studies of 3-aryloylindoles as potent antimitotic agents. *ChemMedChem* **2006**, *1*, 1106–1118.
- Nam, N. H. Combretastatin A-4 analogues as antimitotic anti-tumor agents. *Curr. Med. Chem.* **2003**, *10*, 1697–1722.
- Nguyen, T. L.; McGrath, C.; Hermone, A. R.; Burnett, J. C.; Zaharevitz, D. W.; Day, B. W.; Wipf, P.; Hamel, E.; Gussio, R. A common pharmacophore for a diverse set of colchicine site inhibitors using a structure-based approach. *J. Med. Chem.* **2005**, *48*, 6107–6116.
- Tahir, S. K.; Han, E. K.; Credo, B.; Jae, H. S.; Pienpol, J. A.; Scatena, C. D.; Wu-Wong, J. R.; Frost, D.; Sham, H.; Rosenberg, S. H.; Ng, S. C. A-204197, a new tubulin-binding agent with antimitotic activity in tumor cell lines resistant to known microtubule inhibitors. *Cancer Res.* **2001**, *61*, 5480–5485.
- Lawrence, N. J.; McGown, A. T.; Ducki, S.; Hadfield, J. A. The interaction of chalcones with tubulin. *Anti-Cancer Drug Des.* **2000**, *15*, 135–141.
- Shih, H.; Deng, L.; Carrera, C. J.; Adachi, S.; Cottam, H. B.; Carson, D. A. Rational design, synthesis and structure–activity relationships of antitumor (E)-2-benzylidene-1-tetralones and

- (*E*)-2-benzylidene-1-indanones. *Bioorg. Med. Chem. Lett.* **2000**, *10*, 487–490.
- (20) Chang, J. Y.; Hsieh, H. P.; Chang, C. Y.; Hsu, K. S.; Chiang, Y. F.; Chen, C. M.; Kuo, C. C.; Liou, J. P. 7-Aroyl-aminoindoline-1-sulfonamides as a novel class of potent antitubulin agents. *J. Med. Chem.* **2006**, *49*, 6656–6659.
- (21) Blokhin, A. V.; Yoo, H. D.; Geralds, R. S.; Nagle, D. G.; Gerwick, W. H.; Hamel, E. Characterization of the interaction of the marine cyanobacterial natural product curacin A with the colchicine site of tubulin and initial structure–activity studies with analogues. *Mol. Pharmacol.* **1995**, *48*, 523–531.
- (22) Gastpar, R.; Goldbrunner, M.; Marko, D.; von Angerer, E. Methoxy-substituted 3-formyl-2-phenylindoles inhibit tubulin polymerization. *J. Med. Chem.* **1998**, *41*, 4965–4972.
- (23) Furukawa, T.; Kubota, T.; Hoffman, R. M. Clinical applications of the histoculture drug response assay. *Clin. Cancer Res.* **1995**, *1*, 305–311.
- (24) Robbins, K. T.; Connors, K. M.; Storniolo, A. M.; Hanchett, C.; Hoffman, R. M. Sponge-gel-supported histoculture drug-response assay for head and neck cancer. Correlations with clinical response to cisplatin. *Arch. Otolaryngol. Head Neck Surg.* **1994**, *120*, 288–292.
- (25) Nogales, E.; Wolf, S. G.; Downing, K. H. Structure of the alpha beta tubulin dimer by electron crystallography. *Nature* **1998**, *391*, 199–203.
- (26) Blokhin, A. V.; Yoo, H. D.; Geralds, R. S.; Nagle, D. G.; Gerwick, W. H.; Hamel, E. Characterization of the interaction of the marine cyanobacterial natural product curacin A with the colchicine site of tubulin and initial structure–activity studies with analogues. *Mol. Pharmacol.* **1995**, *48*, 523–531.
- (27) Cushman, M.; Nagarathnam, D.; Gopal, D.; He, H. M.; Lin, C. M.; Hamel, E. Synthesis and evaluation of analogues of (*Z*)-1-(4-methoxyphenyl)-2-(3,4,5-trimethoxyphenyl)ethene as potential cytotoxic and antimitotic agents. *J. Med. Chem.* **1992**, *35*, 2293–2306.
- (28) Gwaltney, S. L.; Imade, H. M.; Barr, K. J.; Li, Q.; Gehrke, L.; Credo, R. B.; Warner, R. B.; Lee, J. Y.; Kovar, P.; Wang, J.; Nukkala, M. A.; Zielinski, N. A.; Frost, D.; Ng, S. C.; Sham, H. L. Novel sulfonate analogues of combretastatin A-4: potent antimitotic agents. *Bioorg. Med. Chem. Lett.* **2001**, *11*, 871–874.
- (29) Pinney, K. G.; Bounds, A. D.; Dingeman, K. M.; Mocharla, V. P.; Pettit, G. R.; Bai, R.; Hamel, E. A new anti-tubulin agent containing the benzo[b]thiophene ring system. *Bioorg. Med. Chem. Lett.* **1999**, *9*, 1081–1086.
- (30) Finlay, G. J.; Baguley, B. C.; Wilson, W. R. A semiautomated microculture method for investigating growth inhibitory effects of cytotoxic compounds on exponentially growing carcinoma cells. *Anal. Biochem.* **1984**, *139*, 272–277.
- (31) Bollag, D. M.; McQueney, P. A.; Zhu, J.; Hensens, O.; Koupal, L.; Liesch, J.; Goetz, M.; Lazarides, E.; Woods, C. M. Epothilones, a new class of microtubule-stabilizing agents with a Taxol-like mechanism of action. *Cancer Res.* **1995**, *55*, 2325–2333.
- (32) Chen, C. T.; Gan, Y.; Au, J. L.; Wientjes, M. G. Androgen-dependent and -independent human prostate xenograft tumors as models for drug activity evaluation. *Cancer Res.* **1998**, *58*, 2777–2783.